# A DATA-DRIVEN PROBABILISTIC LEARNING APPROACH FOR THE PREDICTION OF CONTROLLABLE PITCH PROPELLERS PERFORMANCE

**STEFANO GAGGERO*, ANTONIO COPPEDE*, DIEGO VILLA*, GIULIANO VERNENGO* AND LUCA BONFIGLIO†**

*DITEN, Polytechnic School
University of Genoa
Via Montallegro 1, 16145, Genoa, Italy
e-mail: stefano.gaggero@unige.it; diego.villa@unige.it; giuliano.vernengo@unige.it;
antonio.coppede@edu.unige.it

† MIT-Sea Grant College Program
Massachusetts Institute of Technology
12 Emily St. NW98-180, Cambridge, MA 02139, USA
e-mail: bonfi@mit.edu

**Key words:** Controllable Pitch Propeller, Multi-fidelity, Gaussian Process, Uncertainty Quantification

**Abstract.** The multi-fidelity machine learning framework proposed in this paper leverages a probabilistic approach based on Gaussian Process modeling for the formulation of stochastic response surfaces capable of describing propeller performance for different mission profiles. The proposed multi-fidelity techniques will help coping with the scarcity of high-fidelity measurements by using lower-fidelity numerical predictions. The existing correlation of the multi-fidelity data sets is used to infer high-fidelity measurements from lower fidelity numerical predictions. The probabilistic formulations embedded in Gaussian Process regressions gives the unique opportunity to learn the target functions describing propeller performance at different operating conditions, while quantifying the uncertainty associated to that specific prediction. While the multi-fidelity autoregressive scheme allows to construct high accurate response surfaces using only few experimental data, Uncertainty Quantification (UQ) provides an important metric to asses the quality of the learning process. We demonstrate the capability of the proposed framework to predict the performance of a controllable pitch propeller using few experimental data coming from towing tank experiments and many medium-fidelity predictions obtained using an in-house developed BEM, validated and verified in many previous studies.

## 1 INTRODUCTION AND MOTIVATION

Controllable Pitch Propellers (CPP) offer a propulsion flexibility that is particularly suitable for marine vehicles designed to operate at different mission profiles. Predicting CPP perfor-

mance in a wide range of operating conditions, therefore, is essential for the characterization of the propulsive features of a vessel. Modern propeller design relies on design by optimization techniques in which propeller performance are predicted using low- or medium-fidelity numerical methods, while design assessment is often performed with high-fidelity computational models [1, 2] or, in case of innovative designs, through open-water experiments at the cavitation tunnels [3]. Once the design process converges towards an optimized shape (as in [4, 5]), it is important to characterize CPP propellers for different operating conditions in order to increase the knowledge of the engineering system, predicting possible pitfalls due to performance loss, increase in fuel oil consumption or other important consequences such as excessive loads on the blade, radiated noise [6] or the occurrence of cavitation that could compromise the structural integrity of the propeller. Considering instead an existing, operating, vessel it would be necessary to measure the performance of the propulsion system in a wide range of operating conditions to have its complete characterization. However, in most cases, this might be technically prohibitive and too expensive to be achieved.

In this study we present a mathematical framework capable of constructing accurate surrogate models using only a few high-fidelity data and many numerical predictions performed with inexpensive, low-fidelity computer codes. In this paper we propose a supervised learning framework in which the labeled data coming from two different outputs are blended together using multi-fidelity Gaussian process regression [7, 8, 9, 10, 11, 12]. Multi-fidelity Gaussian Process Regressions have been successfully applied in the naval engineering field for the hydrodynamic and hydro-structural shape optimization of super-cavitating hydrofoils [13, 14] and hull-forms for both calm water resistance [15] and ship motions reduction [16]. Bonfiglio et al. [17] used numerical predictions and experiments to predict hydrodynamic performance of a conventional super-cavitating hydrofoil in the operating conditions input space by leveraging multi-fidelity Gaussian Process Regressions. More simplified multi-fidelity strategies for surrogate model formulations have been recently proposed in [18, 19]. To the best of our knowledge, this is the first time such tools are applied for the predictions of propeller performance in the operating conditions input space.

## 2 GAUSSIAN PROCESS REGRESSIONS

The supervised learning framework proposed in this paper is based on the formulation of probabilistic regression models that are capable of combining multiple sets of data coming from different information sources and providing quantities of interest information at different fidelity levels. In particular, we leverage Gaussian Process $\mathcal{GP}$ regressions in order to model a non-linear function describing the CPP performance in terms of thrust ($K_T$) and torque ($K_Q$) coefficient at different advance coefficients ($J$). In the present paper we demonstrate the main advantages of the proposed framework through a study that involves two different information sources, namely experimental data and numerical predictions. The framework can be extended to an arbitrary number of information sources.

### 2.1 Nonlinear regression with Gaussian processes

The multi-fidelity model proposed in this paper allows to infer high-fidelity predictions by using information mainly provided by lower fidelity models. In this setting, we assume that we

have a data-set comprising of input/output pairs $\mathcal{D} = \{(x_i, y_i)_{i=1}^N\} = \{X, y\}$ where $X$ is a set of given parameters describing the operating conditions of the propeller (e.g. $J$ and $P/D$) and $y$ is their corresponding performance metric (e.g. $K_T$ or $K_Q$). The final goal is to infer a latent function $f$ describing each quantity of interest in terms of nosy input data:

$$y = f(X) + \epsilon. \tag{1}$$

Here $X$ is considered to be a matrix in $\mathbb{R}^{N\times D}$ containing the $N$ input points at which we have observed the outputs $y \in \mathbb{R}^{N\times 1}$. Moreover, $\epsilon$ is a noise process that may be corrupting our observations of $y$. For simplicity, here we assume that $\epsilon$ is Gaussian and uncorrelated, i.e. $\epsilon \sim \mathcal{N}(0, \sigma_n^2 I)$, where $\sigma_n^2$ is an unknown variance parameter that will be learned from the data, 0 is a zero column vector of size $N$, and $I$ is the $N \times N$ identity matrix.

In this study we will consider, without lack of generality, zero-mean Gaussian process priors on $f$, i.e., $f(x) \sim \mathcal{GP}(0, k(x, x'; \theta))$, our goal is to first identify the optimal set of kernel hyper-parameters and model parameters, $\Theta = \{\theta, \sigma_n^2\}$, and then use the optimized model to perform predictions at a set of new unobserved locations $x^*$. A central role in this process is played by the covariance kernel function $k(x, x'; \theta)$ that depends on a set of hyper-parameters $\theta$ and encodes any prior belief or domain expertise we may have about the underlying function $f$. Here, in absence of any domain-specific knowledge we have used the squared exponential covariance kernel.

Model training is performed through minimizing the negative log-marginal likelihood of the Gaussian process model [7]. In our setup, the likelihood is Gaussian and can be computed in a closed analytical form

$$\Theta^* = \arg\min_{\Theta} \mathcal{L}(\Theta) := \frac{1}{2}\log|K + \sigma_n^2 I| + \frac{1}{2} y^T (K + \sigma_n^2 I)^{-1} y + \frac{N}{2}\log(2\pi), \tag{2}$$

where $K$ is a $N \times N$ covariance matrix constructed by evaluating the kernel function $k(\cdot, \cdot; \theta)$ at the locations of the input training data in $X$. The minimization here is carried out using the quasi-Newton optimizer L-BFGS with random restarts [7]. Finally, once the model has been trained on the available data, we can compute the posterior predictive distribution at a new location $x^*$, namely $p(y^*|x^*, \mathcal{D}) \sim \mathcal{N}(\mu(x^*), \Sigma(x^*))$, by conditioning on the observed data as

$$\mu(x^*) = k(x^*, X)(K + \sigma_n^2)^{-1} y \tag{3}$$

$$\Sigma(x^*) = k(x^*, x^*) - k(x^*, X)(K + \sigma_n^2)^{-1} k(X, x^*). \tag{4}$$

Here, we must emphasize the use of Gaussian processes as flexible prior distributions for Bayesian regression of deterministic nonlinear functions. It is well known and understood that Gaussian processes offer a flexible class of prior distributions over function spaces, and provide a concrete formulation for Bayesian non-parametric regression [20]. Under the Central Limit Theorem, one can rigorously prove that Gaussian processes can be obtained as the infinite limits of deep neural networks (i.e., neural networks with multiple layers, an infinite number of neurons per layer, and a Gaussian prior on their weights) [21]. Moreover, rigorous statistical consistency estimates can be obtained using approximation theory in Reproducing Kernel Hilbert Spaces [22]. Therefore, our choice of employing a Gaussian process prior for approximating the non-linear function $f$ in equation 1 is reasonable, as this choice allows us to approximate smooth,

yet arbitrarily complicated functions in high-dimensions. A need for a more complex non-Gaussian prior would only arise in cases where $f$ would have jump discontinuities (leading to a bi-modal distribution of $y$ for a given $x$), or in cases where our observations are corrupted by a non-Gaussian noise process. Such cases are not relevant to our study as our quantities of interest are smooth functions of their inputs, and our observations $y$ are outputs of deterministic computer simulations. Therefore, the reader should hereby note the difference between modeling stochastic phenomena using Gaussian distributions (which is not relevant to this study) versus approximating smooth deterministic functions using Bayesian non-parametric regression with Gaussian process priors, which is the main building block of this study.

The key motivation for adopting a Bayesian approach to approximate deterministic functions stems from the central role played by the quantification of the uncertainty associated with our surrogate model predictions. This uncertainty can reflect both any bias in the training data as well as the uncertainty inherent to the prior modeling assumptions themselves. Besides offering a quantitative mechanism for assessing model inadequacy, this is key to facilitating the judicious acquisition of new information within an optimization loop (see for instance [17]).

### 2.2 Multi-fidelity modeling

The aforementioned work-flow can be straightforwardly extended to handle cases involving data that originate from different information sources of variable fidelity [12, 23, 8]. For simplicity, here we outline the process corresponding to two levels of fidelity, although this can be generalized to arbitrarily many levels. In a two-level multi-fidelity setting we observe data $\mathcal{D} = [\{(x_{L_i}, y_{L_i})_{i=1}^{N_L}\}, \{(x_{H_i}, y_{H_i})_{i=1}^{N_H}\}] = \{X, y\}$, where $(x_L, y_L)$ and $(x_H, y_H)$ are input/output pairs generated by a low- and high-fidelity model, respectively, typically with $N_L >> N_H$. Then, our goal is to set up a multi-variate regression framework that can return accurate high-fidelity predictions while being primarily trained on low-fidelity data. To do so, we consider the following multi-output Gaussian process regression model first put forth by Kennedy and O'Hagan [12]:

$$y_L = f_L(x_L) + \epsilon_L \tag{5}$$
$$y_H = f_H(x_H) + \epsilon_H \tag{6}$$
$$f_H(x) = \rho f_L(x) + \delta(x) \tag{7}$$
$$f_L(x) \sim \mathcal{GP}(0, k_L(x; x'; \theta_L), \qquad \epsilon_L \sim \mathcal{N}(0, \sigma_{n_L}^2 I) \tag{8}$$
$$\delta(x) \sim \mathcal{GP}(0, k_H(x; x'; \theta_H), \qquad \epsilon_H \sim \mathcal{N}(0, \sigma_{n_H}^2 I) \tag{9}$$

Here $f_L(x)$ and $\delta(x)$ are considered to be two independent Gaussian processes, $\rho$ is a scaling parameter that is learned during model training along with the variances $\sigma_{n_L}^2$ and $\sigma_{n_H}^2$ that potentially corrupt the low- and high-fidelity data, respectively. As a consequence of the auto-regressive assumption in Eq. 7, the joint distribution of the low- and high-fidelity data inherits the following structure:

$$y = \begin{bmatrix} y_L \\ y_H \end{bmatrix} \sim \mathcal{N}\left( \begin{bmatrix} 0 \\ 0 \end{bmatrix}, \begin{bmatrix} k_L(x_L, x_L'; \theta_L) + \sigma_{n_L}^2 I & \rho k_L(x_L, x_H'; \theta_L) \\ \rho k_L(x_H, x_L'; \theta_L) & \rho^2 k_L(x_H, x_H'; \theta_L) + k_H(x_H, x_H'; \theta_H) + \sigma_{n_H}^2 I \end{bmatrix} \right) \tag{10}$$

Evidently, the covariance of $y$ now has a block structure, where the diagonal blocks model the data in each fidelity level and the off-diagonal blocks model the cross-correlation structure between different levels of fidelity. Model training and posterior predictions can now be performed by using the concatenated low- and high-fidelity data along with this block covariance matrix structure replacing $K$ in Eq. 2- 4. Specifically, the minimization of the log-marginal likelihood in Eq. 2 will return the optimal set of model parameters and hyper-parameters, namely $\Theta = \{\theta_L, \theta_H, \rho, \sigma^2_{n_L}, \sigma^2_{n_H}\}$, which can be subsequently used to perform posterior predictions using Eq. 3, 4.

## 3 PROPELLER PERFORMANCE DATA SETS

The propeller performance we considered for current analyses are those of the P2772. P2772 is the four-bladed, left-handed controllable pitch propeller of the "Medium Size Tanker" provided in the framework of the European Project AQUO [24]. It has an expanded area ratio of 0.45 and a chord over diameter at $r/R = 0.7$ of 0.29. At the design condition, the pitch over diameter ratio measured at $r/R = 0.7$ is equal to 0.87. Model scale tests are available from SSPA Sweden. Three pitch settings in addition to the design conditions are considered, namely $P/D = 0.9, 0.75$ and 0.6, which correspond to rigid rotations of the propeller blades from $+0.72$ to $-6.6°$.

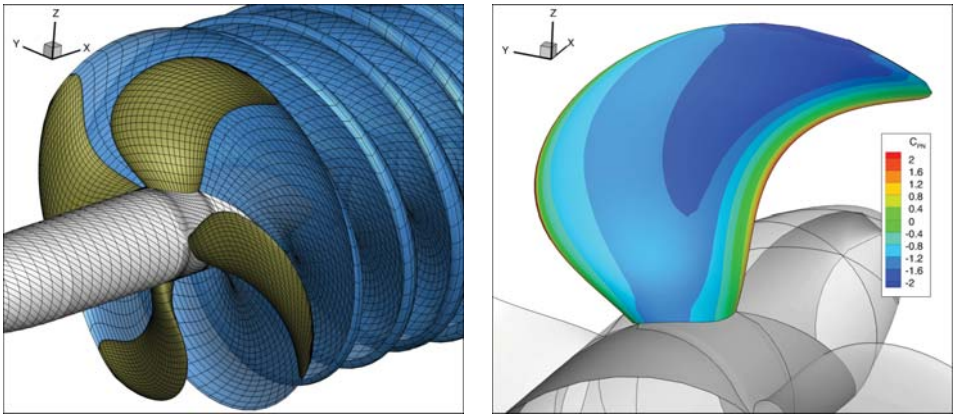


(a) Surface Mesh for BEM calculations

(b) Pressure coefficient distribution ($C_{PN}$) on the key blade. Design pitch at $J = 0.5$

**Figure 1**: The P2772 propeller.

Numerical calculations were carried out using the Boundary Element Methods developed at the University of Genoa [3, 1]. It makes use of the *key blade* approach (figure 1(b)) to solve steady and unsteady problems also in presence of cavitation. In current analyses, we exploit steady, non-cavitating calculations on a blade surface mesh of 1500 panels (figure 1(a)) to characterize the open water performance of the propeller at the same functioning conditions available from experiments. Bollard-pull functioning, at any pitch settings, were not calculated due to the inherent limitations of BEM in dealing with zero inflow speed. Differences between calculations and measurements are reasonable with an average deviation for thrust and torque of about 2% (both overestimated) when the design pitch is considered. At the reduced pitch, instead, calculations significantly underestimate (18% and 15% on average) propeller performance. Moreover, as

highlighted in figures 3(a) and 3(c), also the slope of the thrust and the torque curves computed by the BEM are significantly different from measurements.

## 4 STOCHASTIC SURROGATE MODELS PREDICTIONS

We leverage the data set previously described to construct probabilistic surrogate models describing CPP characteristics at different advance coefficients $J$ and different pitch ratios $P/D$. To demonstrate the capabilities of the multi-fidelity $\mathcal{GP}$ regressions framework proposed in this paper, we first focus on a simplified one-dimensional input space. The input matrix $X$ is defined in $\mathbb{R}^{N_T \times 1}$ where $N_T$ is the number of input points used to train our surrogate models. We have at our disposal $N = 10$ experiments, performed at the SSPA towing tank [24]. The cost of the experimental campaign consists mostly in the construction of the propeller model and set-up of the towing tank, that including the cost of the equipment and the time required for its calibration. Additional experiments at different advance coefficients do not usually cause a significant increase in cost or time. Nevertheless, in this paper we aim at demonstrating the capabilities of the proposed multi-fidelity framework of predicting quantities of interest when high-fidelity measurements are expensive or difficult to obtain. We model our probabilistic surrogates using a zero-mean $\mathcal{GP}$ with a squared exponential covariance function $k$, which in one dimension is defined as follows:

$$k(x_p, x_q) = \sigma_f^2 \exp\left( -\frac{1}{2\ell}|x_p - x_q'|^2 \right) + \sigma_n^2 \delta_{pq} \tag{11}$$

The covariance function depends on three hyper-parameters, representing signal variance $\sigma_f$, length-scale $\ell$ and noise-variance $\sigma_n$. Here we assume noise-free experiments, hence $\sigma_n$=0. Hyperparameters are discovered using the the available data and minimizing the negative log-likelihood, as described in (2). Once the hyper-parameters describing our data-sets are discovered, posterior mean predictions are obtained from (3) and (4), which for thrust coefficient read as follows:

$$\widehat{K_T}(J^*) = k(J^*, J)(K + \sigma_n^2)^{-1} K_T(J) \tag{12}$$

$$\Sigma(J^*) = k(J^*, J^*) - k(J^*, J)(K + \sigma_n^2)^{-1} k(J, J^*). \tag{13}$$

Here the relative $L_2$ error between model prediction $\widehat{K_T}$ and experiments $K_T$ is computed (at the location of the measurements) as follows:

$$\frac{||\widehat{K_T} - K_T||}{||K_T||} = \frac{\sqrt{\sum_{i=1}^{N_V} |\widehat{K_T}(J_i) - K_T(J_i)|^2}}{\sqrt{\sum_{i=1}^{N_V} |K_T(J_i)|^2}} \tag{14}$$

Here $N_V$ is the number of available experiments not including in training ($N_V = N - N_T$).

Figure 2 presents results obtained using $N_T = 3$ (figures 2(a) and 2(b)) and $N_T = 2$ points (figures 2(c) and 2(d)). Each point represent a measurement of thrust and torque obtained an experiment performed at a given advance coefficient $J$.

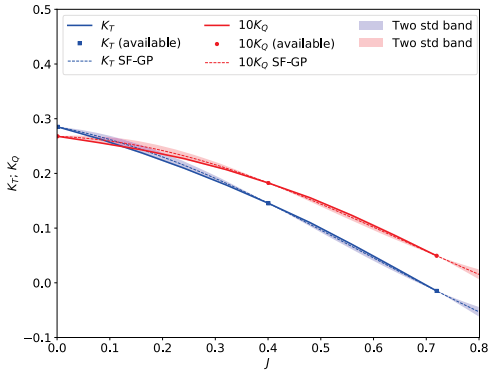


(a) Three Experiments: $J$=0, $J$=0.4, $J$=0.72

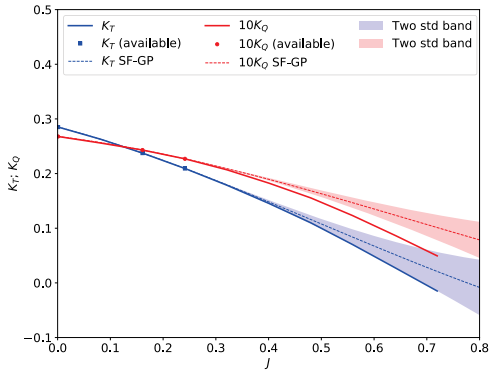


(b) Three Experiments: $J$=0, $J$=0.16, $J$=0.24

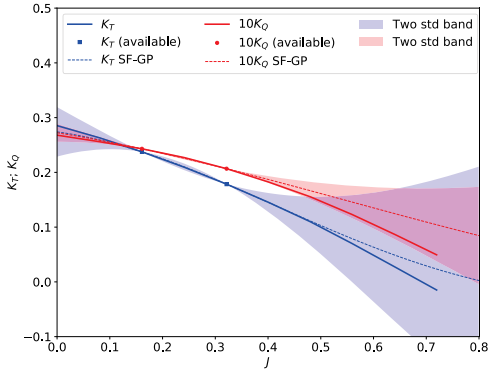


(c) Two Experiments: $J$=0.16, $J$=0.321

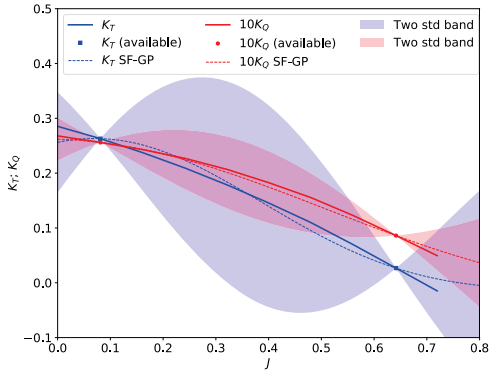


(d) Two Experiments: $J$=0.08, $J$=0.64

**Figure 2**: Construction of single-fidelity $\mathcal{GP}$ regressions for thrust (blue) and torque (red) coefficients in the 1-D input space of advance coefficient $J$. The posterior mean is described by dashed lines, while uncertainty is described by a colored $2\sigma$ band. High-fidelity data used in model training are represented by means of circular dots, while high-fidelity measurements are described by green continuous line. Panels show results obtained for different training data sets.

Figure 2 demonstrates how $\mathcal{GP}$ can accurately approximate thrust and torque at different advance coefficients $J$ if surrogate models are trained using $N = 3$ measurements opportunely selected. In figure 2(a) posterior means (dashed lines in figure 2(a)) approximate experiments with a relative $L_2$ error of 1.96% for $K_T$ and 1.93 for $K_Q$%. As demonstrated in figure 2(a), the accuracy of model predictions is satisfactory in the whole input range $J \in [0, 0.7]$. The maximum uncertainty is located at $J = 0.17$. This is consistent with the location of the experiments used in training: uncertainty becomes larger far from the data and where the function to discover is characterized by higher gradients. Selecting $N = 3$ experiments at different advance coefficients increases the uncertainty and the relative $L_2$ error, as presented in figure 2(b), where we trained surrogate models using only experiments performed at the lowest advance coefficients. Also in this case the uncertainty is higher far from the data, as

**Table 1**: Validation of $\mathcal{GP}$ single-fidelity regressions for different high-fidelity measurements used for model training. Four different cases correspond to different training data sets. Relative $L_2$ error computed at the locations of high-fidelity measurements that were not included in model training, maximum uncertainty ($2\sigma$) and location of maximum uncertainty ($J_{\Sigma_{max}}$) are described for both thrust ($K_T$) and torque ($K_Q$) coefficients. High-fidelity inputs are indicated in terms of advance coefficients in square bracket.

| | $K_T$ | | | $K_Q$ | | |
|---|---|---|---|---|---|---|
| Inputs ($J$) | $L_2$ error | $2\sqrt{\Sigma_{max}}$ | $J_{\Sigma_{max}}$ | $L_2$ error | $2\sqrt{\Sigma_{max}}$ | $J_{\Sigma_{max}}$ |
| [0, 0.40, 0.72] | 1.96% | 0.008 | 0.17 | 1.93 % | 0.008 | 0.17 |
| [0, 0.16, 0.24] | 8.1% | 0.05 | 0.7 | 11.4 % | 0.03 | 0.8 |
| [0.16, 0.321] | 8.2% | 0.15 | 0.7 | 11.7 % | 0.06 | 0.7 |
| [0.08, 0.64] | 8.2% | 0.18 | 0.36 | 3.3% | 0.07 | 0.36 |

.

demonstrated by the $2\sigma$ shaded regions in figure 2(b). When using only $N = 2$ measurements, the quality of model prediction significantly decreases, as showed in figures 2(c) and 2(d). Even if the relative $L_2$ error does not significantly increase, the trend of both thrust and torque coefficient is not correctly captured and the uncertainty associated to surrogate model prediction highlights these discrepancies. Table 1 summarizes results in figure 2 and demonstrates the importance of a strategic selection of training data when constructing probabilistic surrogate models. In many engineering problems quantities of interest can be inferred using prediction models based on simplified physics, numerical approximations or empirical regressions. This is true also for hydrodynamic objective functions characterizing propeller performance. The following examples demonstrate how numerical models, based on the simplified assumption of potential flow, can significantly improve the predictions of open water propeller performance in a wide range of operating conditions. The situation is well represented in figure 3(a) where we have $N_T = 2$ experiments available and low-fidelity predictions available in the entire range of $J$. The accuracy of low-fidelity numerical predictions is qualitatively described in figure 3(a). The relative error between predicted and measured thrust coefficient is as high as 20% at $J = 0.1$. We construct multi-fidelity surrogate models as described in section 2(b). In particular, we use a data set $\mathcal{D}_1 = [\{(J_{L_i}, K_{TL_i})_{i=1}^{N_L}\}, \{(J_{H_i}, K_{TH_i})_{i=1}^{N_H}\}] = \{J, K_T\}$ and $\mathcal{D}_2 = [\{(J_{L_i}, K_{QL_i})_{i=1}^{N_L}\}, \{(J_{H_i}, K_{QH_i})_{i=1}^{N_H}\}] = \{J, K_Q\}$ where $N_L = 7$, $J_L$ is a vector of evenly spaced advance coefficients ($J \in [0.1, 0.7]$) and $N_H = 2$ represents the number of high-fidelity measurements collected during the experimental campaign. The covariance selected for modeling both low- and high-fidelity data, as well as the their cross-correlation is a squared exponential function as described in equation (11).

$$k_L(x_{pL}, x_{qL}) = \sigma_{fL}^2 \exp\left( -\frac{1}{2\ell_L}|x_{pL} - x'_{qL}|^2 \right) + \sigma_{nL}^2 \delta_{pq} \tag{15}$$

$$k_H(x_{pH}, x_{qH}) = \sigma_{fH}^2 \exp\left( -\frac{1}{2\ell_H}|x_{pH} - x'_{qH}|^2 \right) + \sigma_{nH}^2 \delta_{pq} \tag{16}$$

Therefore, a total of 7 hyper-parameters $\Theta = [\sigma_{fL}, \ell_L, \sigma_{nL}, \sigma_{fH}, \ell_H, \sigma_{nH}, \rho]$ will be learned from negative log-likelihood minimization. In the proposed multi-fidelity training, surrogate models are constructed assuming noise-free high-fidelity data and noisy low-fidelity predictions, in which

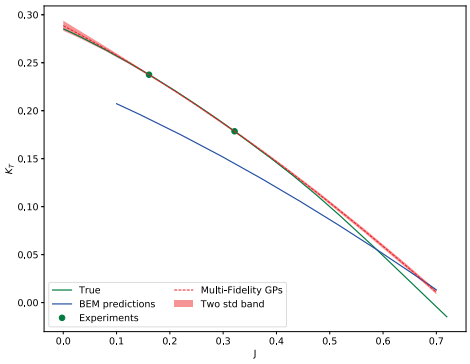


(a) $K_T$ at $J$=0.161, $J$=0.321

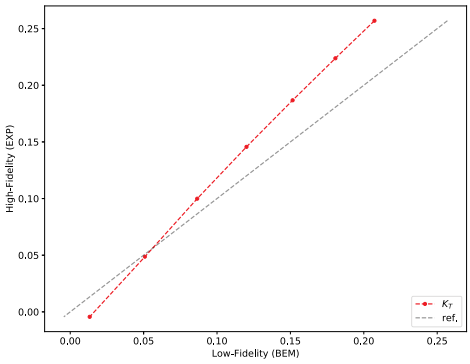


(b) low- high-fidelity correlation

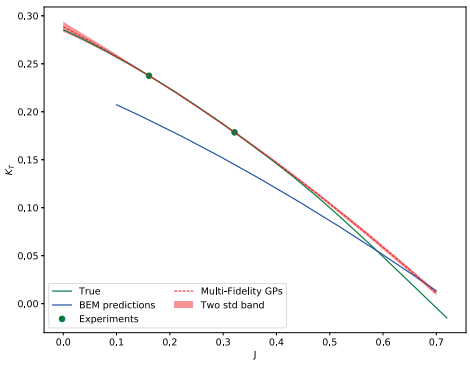


(c) $K_Q$ at $J$=0.161, $J$=0.321

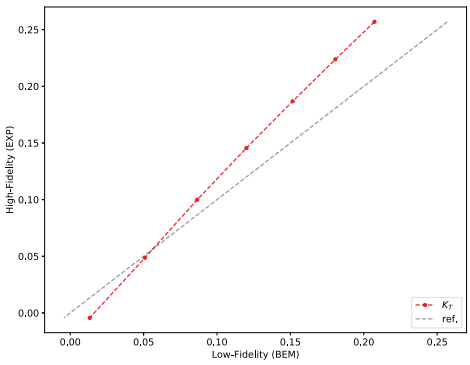


(d) low- high-fidelity correlation

**Figure 3**: Construction of multi-fidelity $\mathcal{GP}$ regressions for thrust and torque coefficients in the 1-D input space of advance coefficient $J$. The posterior mean is described by red dashed line, while uncertainty is described by a $2\sigma$ band colored in red. Low-fidelity data are evenly distributed in the range of $J \in [0, 0.7]$ and they are described with blue continuous line. High-fidelity data used in model training are represented by means of green circular dots, while high-fidelity measurements are described by green continuous line. For each quantity of interest we indicated the correlation between low- (LF) and high-fidelity (HF) data by means of red dashed curve (figures 3(b) and 3(d)). Grey dashed curve represents the situation for which LF=HF.

the noise $\sigma_{nL}$ will be learned from data through negative log-likelihood minimization. Figure 3 presents results obtained for thrust coefficient predictions using $N_L = 7$ low-fidelity numerical predictions and $N_H = 2$ high-fidelity towing tank measurements at $J = 0.16$ and $J = 0.32$. Results in figure 3(a) demonstrate the significant improvements obtained by combining high-fidelity experimental measurements with low-fidelity numerical predictions. Even with low-fidelity predictions characterized by high inaccuracies (20% for $J = 0.1$), the linear correlation between low- and high-fidelity data (showed in figure 3(b)), allows to construct multi-fidelity $\mathcal{GP}$ leveraging the autoregressive assumption expressed in (7). Results presented in figure 3(c) in terms of torque coefficient predictions ($K_Q$) confirms the advantages of the multi-fidelity

**Table 2**: Validation of $\mathcal{GP}$ regressions for different high-fidelity measurements used for model training. Four different cases correspond to many sets of high-fidelity data. For each high-fidelity data set, multi-fidelity surrogates (HF+LF) are compared to single-fidelity models (HF) in terms of relative $L_2$ error computed at the locations of high-fidelity measurements that were not included in model training, maximum uncertainty ($2\sigma$) and location of maximum uncertainty ($J_{\Sigma_{max}}$). Results are presented for both thrust ($K_T$) and torque ($K_Q$) coefficients. High-fidelity inputs are indicated in terms of advance coefficients in square bracket. Low-fidelity inputs are evenly distributed in $J \in [0, 0.7]$.

| | $K_T$ | | | $K_Q$ | | |
|---|---|---|---|---|---|---|
| Inputs ($J$) | $L_2$ error | $2\sqrt{\Sigma_{max}}$ | $J_{\Sigma_{max}}$ | $L_2$ error | $2\sqrt{\Sigma_{max}}$ | $J_{\Sigma_{max}}$ |
| [0, 0.40, 0.72]HF | 1.96% | 0.008 | 0.17 | 1.93 % | 0.008 | 0.17 |
| [0, 0.40, 0.72]HF + LF | 0.26% | 0.002 | 0.18 | 0.54% | 0.0004 | 0.14 |
| [0, 0.16, 0.24]HF | 8.1% | 0.05 | 0.7 | 11.4 % | 0.03 | 0.8 |
| [0, 0.16, 0.24]HF + LF | 3.95% | 0.001 | 0.8 | 4.36 % | 0.0001 | 0.8 |
| [0.16, 0.321]HF | 8.2% | 0.15 | 0.7 | 11.7 % | 0.06 | 0.7 |
| [0.16, 0.321]HF + LF | 3.9% | 0.0005 | 0 | 2.42 % | 0.0006 | 0 |
| [0.08, 0.64]HF | 8.2% | 0.18 | 0.36 | 3.3% | 0.07 | 0.36 |
| [0.08, 0.64]HF + LF | 2.07% | 0.0004 | 0 | 1.13% | 0.0004 | 0 |

framework. In particular, the good accuracy of the posterior mean obtained using high-fidelity data at low advance coefficients is confirmed also at higher $J$. Table 2 presents results obtained using the multi-fidelity framework presented in this study and compares them with single-fidelity modeling. For each high-fidelity data set described in table 1 we trained a multi-fidelity surrogate by blending towing tank measurements with low-fidelity predictions obtained using the BEM previously described. Results in table 2 clearly demonstrate the significant advantages of the multi-fidelity framework.

## 5 CONCLUSIONS

The paper presents a probabilistic approach to predict propeller performance using a diverse pool of data sources. The probabilistic learning framework constructed on the basis of recursive Gaussian Process Regressions is based on a linear autoregressive model. This approach allowed us to seamlessly blend low-fidelity numerical data coming from Boundary Element Method predictions with high-fidelity measurements obtained from cavitation tunnel experiments. In this paper we demonstrate the advantages of the proposed method by constructing surrogate models for open water thrust and torque coefficient of a conventional propeller, for which cavitation tunnel experiments where available at many advance coefficients. However, we validated the proposed framework by considering a limited number of high-fidelity data in the formulation of multi-fidelity $\mathcal{GP}$ models. This demonstrated how the proposed method brings significant advantages if applied to engineering problems characterized by data scarcity such as the performance predictions of full scale propellers on operating vessels.

### Acknowledgements

This project has been partially funded by DARPA EQUiPS grant HR0011517798. Authors wish to thank Prof. G.E. Karniadakis at Brown University for his valuable scientific guidance.

**References**

[1] S. Gaggero, J. Gonzalez-Adalid, and M. P. Sobrino. Design and analysis of a new generation of CLT propellers. *Applied Ocean Research*, 59:424–450, 2016.

[2] S. Gaggero, D. Villa, G. Tani, M. Viviani, and D. Bertetta. Design of Ducted Propeller Nozzles through a RANSE-based optimization approach. *Ocean Engineering*, 145:444–463, 2017.

[3] D. Bertetta, S. Brizzolara, S. Gaggero, M. Viviani, and L. Savio. CPP propeller cavitation and noise optimization at different pitches with panel code and validation by cavitation tunnel measurements. *Ocean engineering*, 53:177–195, 2012.

[4] S. Gaggero, G. Tani, D. Villa, M. Viviani, P. Ausonio, P. Travi, G. Bizzarri, and F. Serra. Efficient and multi-objective cavitating propeller optimization: An application to a high-speed craft. *Applied Ocean Research*, 64:31–57, 2017.

[5] G. Tani, D. Villa, S. Gaggero, M. Viviani, P. Ausonio, P. Travi, G. Bizzarri, and F. Serra. Experimental investigation of pressure pulses and radiated noise for two alternative designs of the propeller of a high-speed craft. *Ocean Engineering*, 132:45–69, 2017.

[6] S. Gaggero, T. Gaggero, E. Rizzuto, G. Tani, D. Villa, M. Viviani, E. Haimov, and J. Hallander. Experimental and numerical investigations for modelling propeller cavitation noise. In Santos T.A. Soares C.G., editor, *Maritime Technology and Engineering - Proceedings of MARTECH 2014: 2nd International Conference on Maritime Technology and Engineering*, pages 695–704. CRC Press/Balkema, 2015.

[7] C. E. Rasmussen and C. K. Williams. In *Gaussian processes for machine learning*, volume 1, chapter 5. MIT press Cambridge, 2006.

[8] P. Perdikaris and G. E. Karniadakis. Model inversion via multi-fidelity Bayesian optimization: a new paradigm for parameter estimation in haemodynamics, and beyond. *Journal of The Royal Society Interface*, 13(118):20151107, 2016.

[9] P. Perdikaris, D. Venturi, J. O. Royset, and G. E. Karniadakis. Multi-fidelity modelling via recursive co-kriging and gaussian–markov random fields. *Proceedings of the Royal Society A: Mathematical, Physical and Engineering Sciences*, 471(2179):20150018, 2015.

[10] L. Le Gratiet and J. Garnier. Recursive co-kriging model for design of computer experiments with multiple levels of fidelity. *International Journal for Uncertainty Quantification*, 4(5):385–386, 2014.

[11] A. Forrester and A. Keane. In *Engineering design via surrogate modeling: a practical guide*, chapter 8. John Wiley & Sons, 2008.

[12] M. C. Kennedy and A. O'Hagan. Predicting the output from a complex computer code when fast approximations are available. *Biometrika*, 87(1):1–13, 2000.

[13] L. Bonfiglio, P. Perdikaris, S. Brizzolara, and G.E. Karniadakis. Multi-fidelity optimization of super-cavitating hydrofoils. *Computer Methods in Applied Mechanics and Engineering*, 332:63–85, 2018.

[14] L. Bonfiglio, P. Perdikaris, J. del Águila, and G. E. Karniadakis. A probabilistic framework for multidisciplinary design: Application to the hydrostructural optimization of supercavitating hydrofoils. *International Journal for Numerical Methods in Engineering*, 116(4):246–269, 2018.

[15] H.C. Raven. Minimising Ship Afterbody Wave Making using Multifidelity Techniques. In *Proceedings of the 32nd Symposium on Naval Hydrodynamics (SNH), August 5-10, 2018, Hamburg, Germany*, 2018.

[16] L. Bonfiglio, P. Perdikaris, G. Vernengo, J. S. de Medeiros, and G. E. Karniadakis. Improving swath seakeeping performance using multi-fidelity gaussian process and bayesian optimization. *Journal of Ship Research*, 62(4):223–240, 2018.

[17] L. Bonfiglio, P. Perdikaris, S. Brizzolara, and G. Karniadakis. A multi-fidelity framework for investigating the performance of super-cavitating hydrofoils under uncertain flow conditions. In *19th AIAA Non-Deterministic Approaches Conference*, page 1328, 2017.

[18] L. Bonfiglio, J. O. Royset, and G. E. Karniadakis. Multi-disciplinary risk-adaptive design of super-cavitating hydrofoil. In *2018 AIAA Non-Deterministic Approaches Conference*, page 1177, 2018.

[19] J. O. Royset, L. Bonfiglio, G. Vernengo, and S. Brizzolara. Risk-adaptive set-based design and applications to shaping a hydrofoil. *Journal of Mechanical Design*, 139(10):101403, 2017.

[20] C. E. Rasmussen. Gaussian processes in machine learning. In *Advanced lectures on machine learning*, pages 63–71. Springer, 2004.

[21] R. M. Neal. Priors for infinite networks. In *Bayesian Learning for Neural Networks*, pages 29–53. Springer, 1996.

[22] A. Stuart and A. Teckentrup. Posterior consistency for gaussian process approximations of bayesian posterior distributions. *Mathematics of Computation*, 87(310):721–753, 2018.

[23] P. Perdikaris, D. Venturi, and G. E. Karniadakis. Multifidelity information fusion algorithms for high-dimensional systems and massive data sets. *SIAM Journal on Scientific Computing*, 38(4):B521–B538, 2016.

[24] AQUO. *Work Package 2: Noise Sources, Task T2.3: Experimental investigations in model scale*. AQUO - Achieve QUieter Oceans by shipping noise footprint reduction, European Commission within the Call FP7, 7th framework program, Grant Agreement no. 314227, 2015.